## Electronic Supplementary Information (ESI)

# Local manipulation of metamagnetism by strain nanopatterning

Michael Foerster, Enric Menéndez, Emerson Coy, Alberto Quintana, Carles Gómez-Olivella, Daniel Esqué de los Ojos, Oriol Vallcorba, Carlos Frontera, Lucia Aballe, Josep Nogués, Jordi Sort,* and Ignasi Fina*

## TABLE OF CONTENTS

# Materials and methods

## Sample growth

55 nm thick FeRh films ($Fe_{50}Rh_{50}$ at. %) are grown on MgO (001) single-crystals. The 5 × 5 $mm^2$ MgO (001) single-crystal substrate is fixed to the sample holder of the sputtering chamber using Ag paste and heated up to the deposition temperature $T_D$ = 300°C in a base pressure of 0.01 mbar of Ar. The FeRh film is then grown by DC magnetron sputtering using 20 W power at a rate of 0.8 Å $s^{-1}$ from a stoichiometric target. Afterwards, the film is annealed at $T_A$ = 700°C in a pressure of 0.1 mbar of Ar for $t_A$ = 1 h and subsequently cooled down to room temperature at a 100°C $min^{-1}$ rate. Finally, at room temperature, a thin 5 nm $AlO_x$ layer is deposited to prevent oxidation.

## Nanoindentation and atomic force microscopy experiments

Nanoindentations are carried out by a UMIS equipment from Fischer Cripps Laboratories for data shown in Figure 2 and a triboindenter TI-950 from Hysitron for data shown in Figures 3, working with a Berkovich diamond tip. Indentations are made using a constant strain (either at 10, 20, 50 or 300 mN) loading and holding time of 1.5 seconds. Long period of drift correction are allowed until the drift is below 0.5 nm $s^{-1}$. The reduced Young's modulus and hardness values are extracted from the load-displacement curves using the methods of Oliver-Pharr.[1] (Supplementary Figure S6) and are in agreement with literature values.[2] Detailed explanation of the methodology and fitting functions can be found elsewhere.[3] The surface morphology of the films is evaluated using the indenter atomic force microscopy option, and the Berkovich tip as a probe. The surface topography measurements of the pre- and post-indent films are collected using a contact load of 0.8 μN, with a scan rate of 0.2 Hz.

## Simulations

Finite element modeling is performed using the ABAQUS software and using the mechanical parameters for FeRh from Ref. 2.

## X-ray characterization

X-ray diffraction measurements are done at the MSPD beamline (ALBA synchrotron).[4] This end-station is equipped with Kirkpatrick-Baez mirrors and a Roayonix SC165 CCD detector. The energy used for the measurements is 29.2 keV ($\lambda$ = 0.42460 Å) determined by the Sn absorption K-edge and the distance and beam center position are calibrated by means of the d2Dplot software using the diffraction of a standard $LaB_6$ sample. Measurements are carried out in transmission through the substrate and scans are performed by rotating the sample around vertical axis. [5]

## Macroscopic magnetic characterization

Magnetization versus temperature characteristics are measured using a vibrating sample magnetometer platform from LOT-Quantum Design applying a magnetic field H = 500 Oe, along the in-plane [100]-MgO direction.

## Magneto-optic Kerr effect characterization

The evolution of the local magnetic properties is investigated using a longitudinal magneto-optic Kerr effect (MOKE) apparatus from Durham Magneto Optics. Longitudinal MOKE measurements are recorded at various temperatures, by applying an in-plane magnetic field (H < 375 Oe) and measuring the Kerr rotation, $\Theta_K$, while heating and cooling the FeRh film.

## XMCD-PEEM characterization

XMCD–PEEM experiments are performed at the CIRCE beamline of the ALBA Synchrotron[6] using circularly polarized x-rays with an energy resolution of $E/\Delta E \approx 5000$. All images are recorded using low energy secondary electrons emitted by X-rays tuned to the Fe $L_3$ absorption edge at ca. 707 eV.

Clock-wise (CW) and counter-clock-wise (CCW) circularly polarized x-rays are used to illuminate the sample, which emits electrons that are imaged by the PEEM detector. From the subtraction of images collected for opposite polarization, the magnetic contrast XMCD–PEEM images are obtained. As indicated in Figure 2(a), black and white areas in the images account respectively for domains with net magnetization along and opposite to the direction of the incident light. Grey regions can account for either domains without net magnetization (here AFM domains), or domains with net magnetization perpendicular to the incident light. Magnetic contrast of the XMCD-PEEM images in regions with domains can be estimated by the standard deviation of the pixelwise intensity ($SD_{XMCD}$) with respect to the mean value.

## Electric transport characterization

The resistance versus temperature measurements is performed in a 4-points configuration with a constant injected current of 100 $\mu$A while cooling/warming the sample at 2°C min$^{-1}$. Namely, 4 gold pads, two on each side of the indented region, are evaporated to perform transport measurements in the 4-points configuration, as shown in Figure 3c. The current is injected and the voltage is measured according to the labels in Figure 3c.

## Electronic Supplementary Information S1

Reciprocal space maps of several reflections are shown in S1a-l. In Figure S1k, the q2 as a function of h,k,l is shown. The q-peak position value is obtained from Gaussian fitting of different reflections shown in Supporting Information Figure S2. The plane q2 = k2/c2+(h2+k2)/a2 (blue) that better matches with the q2 values is that corresponding to a = 2.98 Å and c = 2.99 Å lattice parameter, indicating that the FeRh cell suffers an slight tetragonal distortion compared to its bulk values.[7]

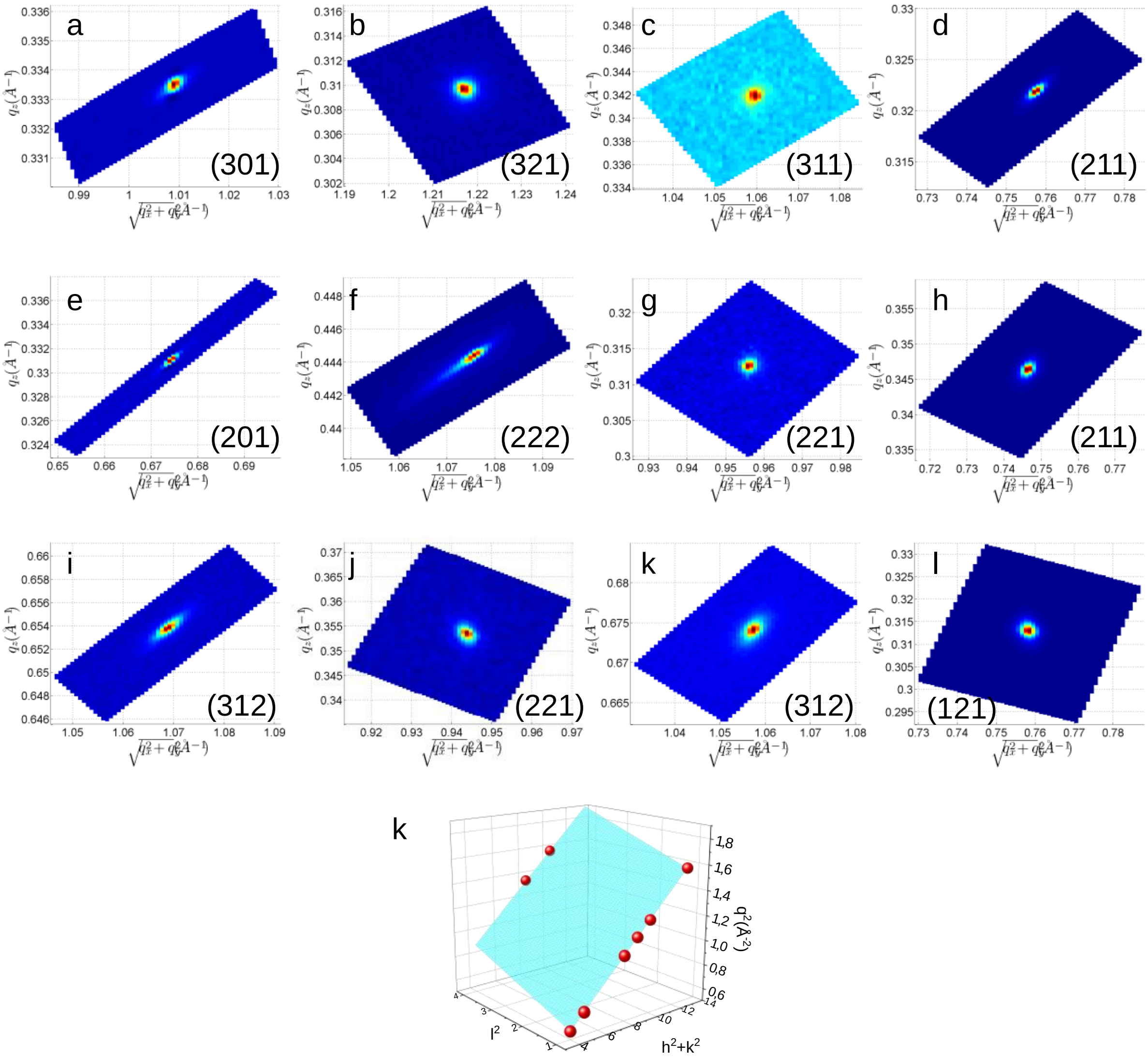


**Figure S1.** (a-l) Reciprocal space map of the indicated reflections. (k) $q^2$ as a function of $l^2$ and $h^2+k^2$. The turquoise-colored plane corresponds to $q^2 = k^2/c^2+(h^2+k^2)/a^2$ with $a$ = 2.98(1) Å and $c$ = 2.99(1) Å.

## Electronic Supplementary Information S2

Fittings Reciprocal space map of Figure S1 are shown in Figure S2.

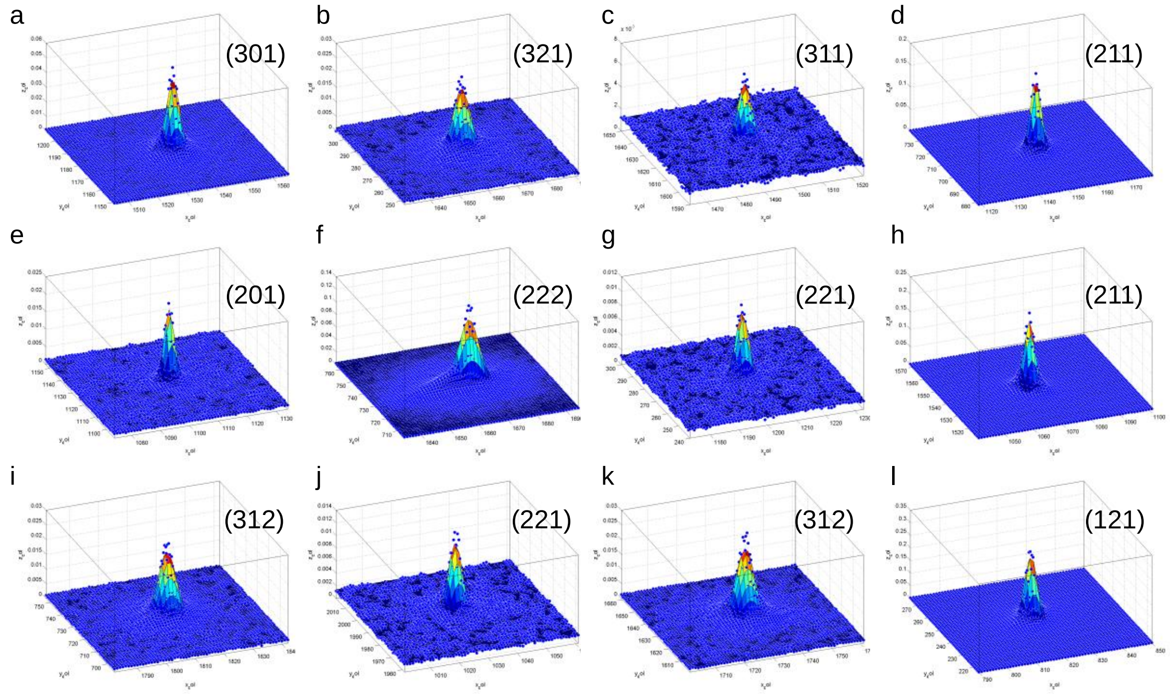


**Figure S2.** (a-l) Reciprocal space map of the indicated reflections. Blue points correspond to measured data and the surface contour corresponds to Gaussian fits. The maxima of the Gaussian fits have been taken as the central point to calculate the lattice parameters given in the main manuscript.

## Electronic Supplementary Information S3

Figure S3 shows the Load-displacement curve performed with a maximum load of 10 mN. The pop-in jump indicates that the MgO substrate is reached and some fracture/cracks have been produced.

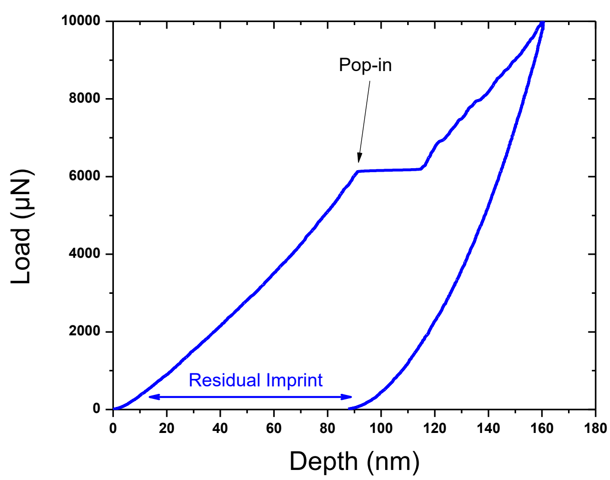


**Figure S3.** Load-displacement nanoindentation curve using a maximum load of 10 mN. The pop-in jump indicates that the MgO substrate is reached and some fracture/cracks have been produced.

## Electronic Supplementary Information S4

Figure S4 shows the arrays of indentations are performed with a maximum load of 5 mN, 10 mN and 20 mN, respectively, from bottom to top.

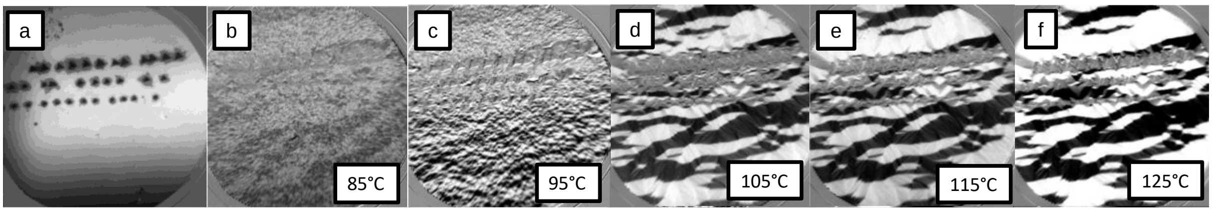


**Figure S4.** (a) PEEM image and (b,c,d,e,f) XMCD-PEEM images as a function of temperature for lines of indentations of different sizes. The arrays of indentations are performed with a maximum load of 5 mN, 10 mN and 20 mN, respectively, from bottom to top.

## Electronic Supplementary Information S5

The calculations to produce the deformation maps of Figure S5 have been done for a Berkovich tip using literature values for the mechanical parameters of the FeRh film,[2] which are similar to the ones obtained experimentally (see Supporting Information Figure S6). Panel a shows an important compression (blue region) at the surface along the [110], [1-10], [-110] and [-1-10] directions (dashed yellow line). In the indented region the compression is maximum in the green/yellow regions.

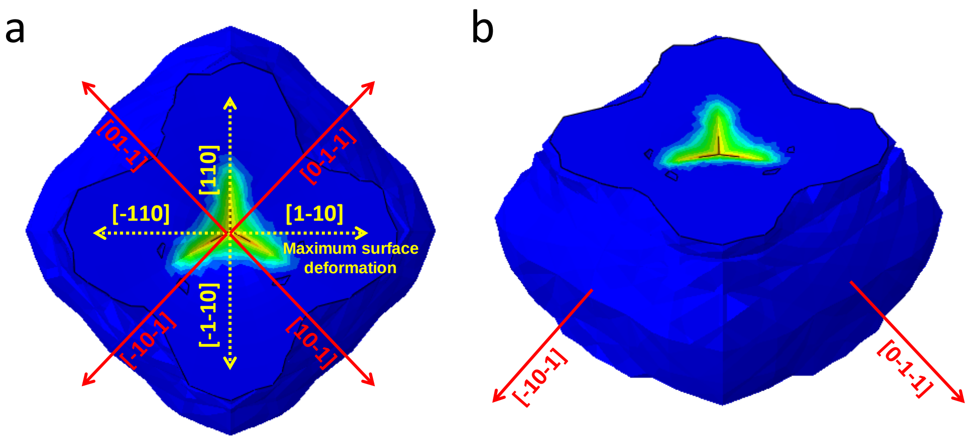


**Figure S5.** Deformation map for a FeRh film calculated using finite-element model: (a) azimuthal and (b) tilted views of the deformation map.

## Electronic Supplementary Information S6

Figure S6 shows the Load-displacement curve used to calculate the mechanical values used to corraborate those used in the calculations shown in Figure S5.

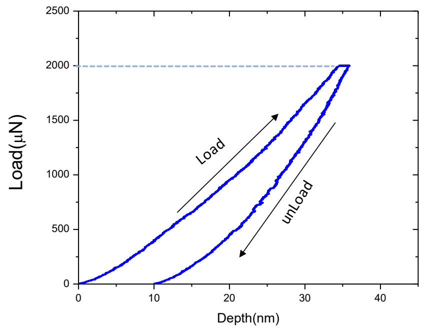


**Figure S6.** Load-displacement nanoindentation curve corresponding to a maximum load of 2 mN. From the curve a reduced Young's modulus of 265 ± 20 GPa and hardness of 8.7 ± 0.8 GPa have been extracted.

## Electronic Supplementary Information S7

Similar simulations to those shown in ESI S5 are shown in Figure S7 for a virtually harder FeRh film. It can be observed that in this case the maximum deformation is found near the edges of the indentation and that it has a 3-fold symmetry in agreement with the results show in Figure 2d and sketched in Figure 2f. This indicate that near the indentation the high temperature XMCD-PEEM images reveal a more relevant role of FeRh strain to that found at intermediate temperatures far from the indentation.

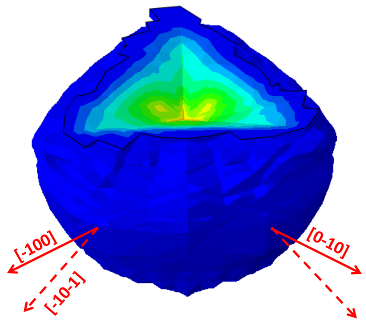


**Figure S7.** Deformation map for a virtually harder FeRh film calculated using finite-element model.

## Electronic Supplementary Information S8

As can be seen in the sequence of images of Figure S8, the local changes of the FeRh FM-AFM transition induced by the indentation show several different remarkable features on different distance scales: i) in the close proximity (1-3 μm) of the indentation and for all temperatures —most easily visible at higher temperatures, corresponding to panels d,e— there are three lobes of gray contrast, centered at the sides of the indentation. This "near field" feature reflects the highest *T** increase (i.e., no transition is observed up to 115ºC), and thus strongest compressive strain, shows a three-fold symmetry, reflecting the triangular shape of pyramidal indentation imprint. ii) At low temperatures (in images a,b) the most prominent feature are four emerging lines of strong FM contrast, originating at the corners of the indentation and protruding for a large distance (ca. 7-8 μm) along the [110] FeRh-directions. Although they originate at the corners of the triangular indentation, they show a clear four-fold symmetry. Remarkably, here *T** appears to be effectively lowered with respect to the rest of the (non-indented) film, indicating an expansive strain. iii) At intermediate temperature (panel c), four rather large (> 5 μm) lobes of gray contrast are observed along the [100] family of directions of FeRh. In summary, the images reveal near-field three-fold areas of strongly compressive strain and far-field, four fold areas of mainly compressive along [110] type of FeRh.

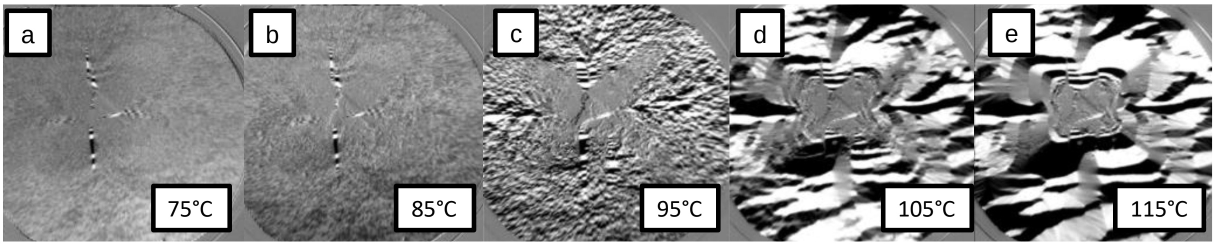


**Figure S8.** (a-e) XMCD-PEEM contrast evolution as a function of temperature (as indicated in the different panels).

## Electronic Supplementary Information References

1. W. C. Oliver and G. M. Pharr, *J. Mater. Res.*, 2004, **19**, 3-20.
2. U. Aschauer, R. Braddell, S. A. Brechbühl, P. M. Derlet and N. A. Spaldin, *Phys. Rev. B*, 2016, **94**, 014109.
3. E. Coy, L. Yate, Z. Kabacińska, M. Jancelewicz, S. Jurga and I. Iatsunskyi, *Mater. Des.*, 2016, **111**, 584-591.
4. F. Fauth, I. Peral, C. Popescu and M. Knapp, *Powder Diffr.*, 2013, **28**, S360-S370.
5. O. Vallcorba and J. Rius, *J. Appl. Crystallogr.*, 2019, **52**, 478.
6. L. Aballe, M. Foerster, E. Pellegrin, J. Nicolas and S. Ferrer, *J. Synchrotron Radiat.*, 2015, **22**, 745-752.
7. A. Zakharov, A. Kadomtseva, R. Levitin and E. Ponyatovskii, *Sov. Phys. JETP*, 1964, **19**, 1348-1353.